CHINESE OPTICS LETTERS

Vol. 22, No. 2 | February 2024

Simultaneously detecting transversal and longitudinal displacement with the dielectric metasurface

Zhiyu Zhang (张植宇)[1], Chenghui Kuang (匡程辉)[1], Haofeng Zang (臧昊峰)[1], Yonghua Lu (鲁拥华)[1,2*], and Pei Wang (王 沛)[1,2]

[1] Department of Optics and Optical Engineering, University of Science and Technology of China, Hefei 230026, China

[2] Advanced Laser Technology Laboratory of Anhui Province, Hefei 230026, China

*Corresponding author: yhlu@ustc.edu.cn

Received July 13, 2023 | Accepted October 7, 2023 | Posted Online February 20, 2024

The compact, sensitive, and multidimensional displacement measurement device plays a crucial role in semiconductor manufacture and high-resolution optical imaging. The metasurface offers a promising solution to develop high-precision displacement metrology. In this work, we proposed and experimentally demonstrated a two-dimensional displacement (*XZ*) measurement device by a dielectric metasurface. Both transversal and longitudinal displacements of the metasurface can be obtained by the analysis of the interference optical intensity that is generated by the deflected light beams while the metasurface is under linearly polarized incidence. We experimentally demonstrated that displacements down to 5.4 nm along the *x*-axis and 0.12 μm along the *z*-axis can be resolved with a 900 μm × 900 μm metasurface. Our work opens up new possibilities to develop a compact high-precision multidimensional displacement sensor.

Keywords: metasurface; transversal and longitudinal displacement measurement.
DOI: 10.3788/COL202422.021202

1. Introduction

High-precision displacement sensing is greatly demanded in diverse fields including semiconductor manufacturing, mechanical engineering, and high-resolution optical imaging[1-4]. The recent progress of nano-optics makes it feasible to develop a compact displacement sensor with accuracy down to the sub-nanometer. Several compact devices[5-10] have been proposed for transversal position sensing, such as collecting highly position-dependent directional scattering from an optical antenna[5,6], utilizing modulated structure light interference[7], and employing super-oscillatory fields[8]. Recently, a polarization-encoded metasurface was used to realize one-dimensional lateral displacement measurement with subnanometric resolution over an enormous range[11,12], providing a new avenue for using the metasurface for displacement sensing. Additionally, simultaneous in- and out-of-plane displacement measurement techniques, such as digital holographic interferometry[13,14] and fringe projection[15], are in great demand for establishing the shape of objects, metrology, and other mechanical applications[16-18]. An ultra-precision heterodyne optical encoder system has also been proposed for *xz*-plane displacement measurement using a linear interferometer[19]. However, achieving compactness and direct readout has proven challenging for these approaches. Therefore, it is also required to develop a simple device to detect transversal and longitudinal displacement simultaneously.

In this Letter, we present a novel approach using a dielectric metasurface to achieve high accuracy in transversal and longitudinal displacement measurement simultaneously. A metasurface that consists of nanopillars rotating in one direction and remaining identical in the other direction is proposed to split the incident light into three beams in different directions and polarizations. Both transversal and longitudinal relative displacements between two adjacent metasurfaces are carried by the phase delay of the deflected light passing through the first metasurface and can be retrieved from the deflected interference light after the second metasurface. We have experimentally demonstrated such two-dimensional displacement measurement with an equivalent setup based on a single metasurface using a reflective 4f-system. Sensitivity and resolution of both the transversal and longitudinal displacements are also evaluated and discussed.

2. Design of the Transversal and Longitudinal Displacement Measurement Metasurface

The schematic diagram in Fig. 1 illustrates the functionality of the paired metasurfaces and the principle of simultaneously detecting transversal and longitudinal displacement between them. A linearly polarized (LP) incident light $\boldsymbol{E}_{\text{in}}$ passes through the first metasurface and splits to three beams, namely $\boldsymbol{E}_{+1}$, $\boldsymbol{E}_{0}$,

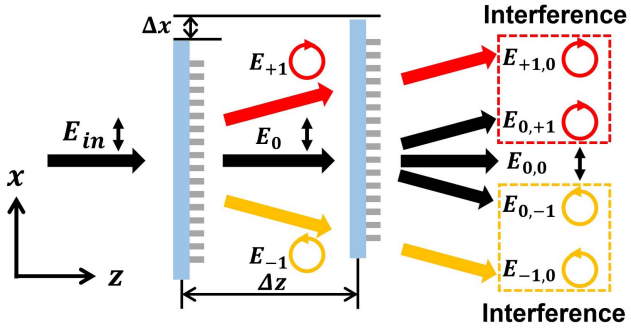

Fig. 1. Schematic diagram of the transversal and longitudinal displacement measurement by two identical metasurfaces. The double arrow represents linear polarization, and the arrowed circles represent the right-handed circular polarization and left-handed circular polarization.

$\boldsymbol{E}_{-1}$, in different directions. The transmitted light $\boldsymbol{E}_0$ maintains the propagating direction and polarization of incident light. The transmitted beams $\boldsymbol{E}_{+1}$ and $\boldsymbol{E}_{-1}$ are in right-handed circular polarization (RCP) and left-handed circular polarization (LCP) and are deflected upward and downward, respectively. Subsequently, the light beam $\boldsymbol{E}_0$ passing through the second metasurface further splits into three beams $\boldsymbol{E}_{0,+1}$, $\boldsymbol{E}_{0,0}$, and $\boldsymbol{E}_{0,-1}$. Additionally, a portion of the $\boldsymbol{E}_{+1}$ and $\boldsymbol{E}_{-1}$ light beams directly passing through the second metasurface can maintain their propagating direction and polarization, designated as $\boldsymbol{E}_{+1,0}$ and $\boldsymbol{E}_{-1,0}$. Thereafter, transmitted light $\boldsymbol{E}_{0,+1}$ and $\boldsymbol{E}_{+1,0}$ (or the $\boldsymbol{E}_{0,-1}$ and $\boldsymbol{E}_{-1,0}$) are both RCP (LCP) and are in the same propagating direction, leading to coherent superposition together. The relative transversal and longitudinal position information of two metasurfaces can be accurately retrieved from the interference intensity.

The Jones matrix function[20,21] can be used to describe the functionalities of metasurface including both polarization conversion and deflection, which can be expressed as

$$\boldsymbol{J}(x) = \eta_1 \boldsymbol{I} + \eta_2 (e^{ik_x x}|R\rangle\langle L| + e^{-ik_x x}|L\rangle\langle R|), \tag{1}$$

where $\boldsymbol{I}$ is a 2×2 identity matrix indicating the transmitted light that maintains the incident direction and polarization, while η_1 is the complex modulation coefficient that represents the amplitude and the phase of transmitted light that maintains the incident direction and polarization. Reciprocally, η_2 represents the complex polarization conversion coefficient. The terms involving $e^{ik_x x}$ and $e^{-ik_x x}$ introduce a linear gradient phase along the x-axis, indicating light deflection away from the incident propagation direction. The deflection angle can be obtained by $\alpha = \arcsin(k_x/k)$, where k is the wave vector of incident light. The kets $|R\rangle = (1, -i)^T/\sqrt{2}$ and $|L\rangle = (1, i)^T/\sqrt{2}$ denote RCP and LCP light, respectively. $|R\rangle\langle L|$ and $|L\rangle\langle R|$ refer to the conversion between RCP and LCP.

When x-polarized incident light, expressed as $|\boldsymbol{E}_{\text{in}}\rangle = \frac{1}{\sqrt{2}}(|R\rangle + |L\rangle)$, illuminates the metasurface, the wavefront after the incident light passes through the first metasurface can be obtained by $|\boldsymbol{E}_{\text{out1}}(x)\rangle = \boldsymbol{J}_1(x)|\boldsymbol{E}_{\text{in}}\rangle$. Considering the wavefront as the transmitted light propagates to a position (x, z), the optical wave function of transmitted light can be applied as

$$|\boldsymbol{E}_{\text{out1}}(x,z)\rangle = \eta_1 e^{ikz}|\boldsymbol{E}_{\text{in}}\rangle + \frac{1}{\sqrt{2}}\eta_2 e^{ik_z z}(e^{-ik_x x}|L\rangle + e^{ik_x x}|R\rangle). \tag{2}$$

Here, the first term represents the $\boldsymbol{E}_0$ light beam with the same polarization and propagating direction as the incident light. The second and the third terms are deflected light beams $\boldsymbol{E}_{+1}$ and $\boldsymbol{E}_{-1}$ in RCP and LCP, respectively. $k_z = \sqrt{k^2 - k_x^2}$ is the wave vector along the z axis for the deflected transmitted light. Subsequently, the transmitted light passes through the second metasurface. A transversal separation Δx and a longitudinal separation Δz are introduced as the displacement to describe the relative position of two metasurfaces. Then, the wavefront after passing through the second metasurfacce can be obtained as $|\boldsymbol{E}_{\text{out2}}(x)\rangle = \boldsymbol{J}_2(x + \Delta x)|\boldsymbol{E}_{\text{out1}}(x, \Delta z)\rangle$. In detail, the $\boldsymbol{E}_0$ transmitted light further splits to three beams as

$$\begin{cases} \boldsymbol{E}_{0,+1} = \frac{1}{\sqrt{2}}\eta_1\eta_2 e^{i(k\Delta z + k_x \Delta x)} e^{ik_x x}|R\rangle, \\ \boldsymbol{E}_{0,0} = \eta_1^2 e^{ik\Delta z}|\boldsymbol{E}_{\text{in}}\rangle, \\ \boldsymbol{E}_{0,-1} = \frac{1}{\sqrt{2}}\eta_1\eta_2 e^{i(k\Delta z - k_x \Delta x)} e^{-ik_x x}|L\rangle. \end{cases} \tag{3}$$

A portion of $\boldsymbol{E}_{+1}$ and $\boldsymbol{E}_{-1}$ directly passes through the second metasurface and is modulated by η_1, which can be expressed as

$$\begin{cases} \boldsymbol{E}_{+1,0} = \frac{1}{\sqrt{2}}\eta_1\eta_2 e^{ik_z \Delta z} e^{ik_x x}|R\rangle, \\ \boldsymbol{E}_{-1,0} = \frac{1}{\sqrt{2}}\eta_1\eta_2 e^{ik_z \Delta z} e^{-ik_x x}|L\rangle. \end{cases} \tag{4}$$

It is obvious that $\boldsymbol{E}_{0,+1}$ and $\boldsymbol{E}_{+1,0}$ (or $\boldsymbol{E}_{0,-1}$ and $\boldsymbol{E}_{-1,0}$) have identical parts $e^{ik_x x}|R\rangle$ $(e^{-ik_x x}|L\rangle)$, indicating the same polarization and propagation direction. Therefore, optical interference occurs. The interference intensity can be calculated as

$$\begin{cases} \boldsymbol{I}_{+1} &= |\boldsymbol{E}_{0,+1} + \boldsymbol{E}_{+1,0}|^2 \\ &= |\eta_1|^2|\eta_2|^2\{1 - \cos[(k - k_z)\Delta z + k_x \Delta x]\}, \\ \boldsymbol{I}_{-1} &= |\boldsymbol{E}_{0,-1} + \boldsymbol{E}_{-1,0}|^2 \\ &= |\eta_1|^2|\eta_2|^2\{1 - \cos[(k - k_z)\Delta z - k_x \Delta x]\}. \end{cases} \tag{5}$$

It is clear that the interference intensity varies periodically with respect to the displacement Δz and Δx. It is worth noting that η_1 and η_2 only affect the intensity of the output light, which can be normalized. By analyzing the phase of the normalized intensity, the displacement information can be obtained directly as

$$\begin{cases} \Delta x = \frac{1}{2k_x}[\arccos(1 - 2I_{+1}) - \arccos(1 - 2I_{-1})], \\ \Delta z = \frac{1}{2(k - k_z)}[\arccos(1 - 2I_{+1}) + \arccos(1 - 2I_{-1})]. \end{cases} \tag{6}$$

Therefore, simultaneously detecting transversal and longitudinal displacement can be achieved by measuring the interference intensities of ±1st order output light.

3. Simulated and Experimental Results of the Displacement Measurement Metasurface

The designed metasurface consists of arrayed subwavelength nanopillars with spatially varying optical axis θ (x) along the x-axis. Figures 2(a) and 2(b) present the oblique and top view of a unit cell composed of an elliptical amorphous silicon cylinder on the fused quartz substrate. The optical properties of the unit cell can be described by Jones matrix as[22]

$$\boldsymbol{J}(\theta)=\frac{1}{2}(\tilde{t}_o+\tilde{t}_e)\boldsymbol{I}+\frac{1}{2}(\tilde{t}_o-\tilde{t}_e)(e^{i2\theta}|R\rangle\langle L|+e^{-i2\theta}|L\rangle\langle R|). \quad (7)$$

Here, $\tilde{t}_o=t_o e^{i\varphi_o}$ and $\tilde{t}_e=t_e e^{i\varphi_e}$, where t_o and t_e are amplitude transmittance, and φ_o and φ_e are the phase delay for the incidence along the o-axis and e-axis, respectively. θ is the orientation angle of the major axis of the nanopillar. Compared with Eq. (1), the co-polarized modulation coefficient and polarization conversion coefficient can be expressed as $\eta_1=\frac{1}{2}(\tilde{t}_o+\tilde{t}_e)$ and $\eta_2=\frac{1}{2}(\tilde{t}_o-\tilde{t}_e)$, respectively. The Pancharatnam–Berry (PB) phase $e^{\pm i2\theta}$ can introduce a linear gradient phase $e^{\pm ik_x x}$ if the orientation angle varies along the x-axis as $\theta(x)=\frac{1}{2}k_x x$[20]. To obtain maximum optical intensity of the deflected light $|\eta_1|^2|\eta_2|^2$, a quarter-wave plate condition should be satisfied as

$$\begin{cases} t_o=t_e=1, \\ |\varphi_o-\varphi_e|=\pi/2. \end{cases} \quad (8)$$

In this condition, the ratio of the intensity of 0th order spot $|\boldsymbol{E}_0|^2$ to the intensity of ±1st order spots $|\boldsymbol{E}_{\pm1}|^2$ in Eq. (2) can be calculated as 2 : 1.

To obtain suitable parameters of the nanopillars, we simulated the amplitude transmittance t_o and phase delay φ_o as a function of the major and minor lengths of nanopillars D_o and D_e at wavelength $\lambda=633$ nm, as shown in Figs. 2(c) and 2(d). The period of the nanopillar is set at $P=300$ nm, and the height of the nanopillar is $H=410$ nm. The plots of Figs. 2(c) and 2(d) will represent t_e and φ_e by exchanging D_o and D_e. Consequently, the corresponding $|\eta_1|^2|\eta_2|^2$ for each nanopillar can be calculated as shown in Fig. 2(e). The maximum $|\eta_1|^2|\eta_2|^2$ can be obtained at the position marked by the red dashed ellipse, which also exhibits well tolerance in the size of the structure. Therefore, the nanopillar parameters are optimized as $D_o=194$ nm and $D_e=86$ nm, where $|\eta_1|^2|\eta_2|^2=0.205$. The parameters of the nanopillar also can be further optimized by using artificial intelligence methods to improve the efficiency wideband characteristics of the metasurface[23-25].

Subsequently, we simulated a 30 μm × 30 μm metasurface with $k_x=2\pi/\Lambda$, where $\Lambda=6$ μm is the spatial period of the optical axis of nanopillars. Figure 2(f) presents the far-field intensity distribution of the transmitted light, clearly indicating three spots $\boldsymbol{E}_{+1}$, $\boldsymbol{E}_0$, and $\boldsymbol{E}_{-1}$ corresponding to different propagating directions. The deflection angle of $\boldsymbol{E}_{\pm1}$ beams can be calculated as $\alpha=\arcsin(k_x/k)=6.056^\circ$, which is well consistent with the simulated result. The inset shows the intensity distribution profile along the x axis, where the intensity of $\boldsymbol{E}_0$ spot is twice as much as the intensity of $\boldsymbol{E}_{\pm1}$ spots as predicted.

A 900 μm × 900 μm metasurface with $\Lambda=6$ μm is fabricated by the standard electric beam lithography process. Figure 3(a) illustrates the experimental setup for the displacement measurement. The light from a solid-state laser passes through a linear polarizer and then illuminates the metasurface. The metasurface is placed on a piezo-stage, which allows precision control over the transversal displacement Δx and the longitudinal displacement Δz. The inset in Fig. 3(a) displays the typical scanning electron microscope (SEM) images of the fabricated sample, illustrating the well-controlled geometric size and orientation of nanopillars. After passing through the metasurface, the incident light is divided into $\boldsymbol{E}_{+1}$, $\boldsymbol{E}_0$, and $\boldsymbol{E}_{-1}$ three light beams and then is reflected back to the metasurface using a reflection-type 4f-system. A quarter-wave plate is inserted before the mirror to avoid polarization handedness conversion caused by the mirror reflection. Two intensity signals of the deflected −1st and +1st

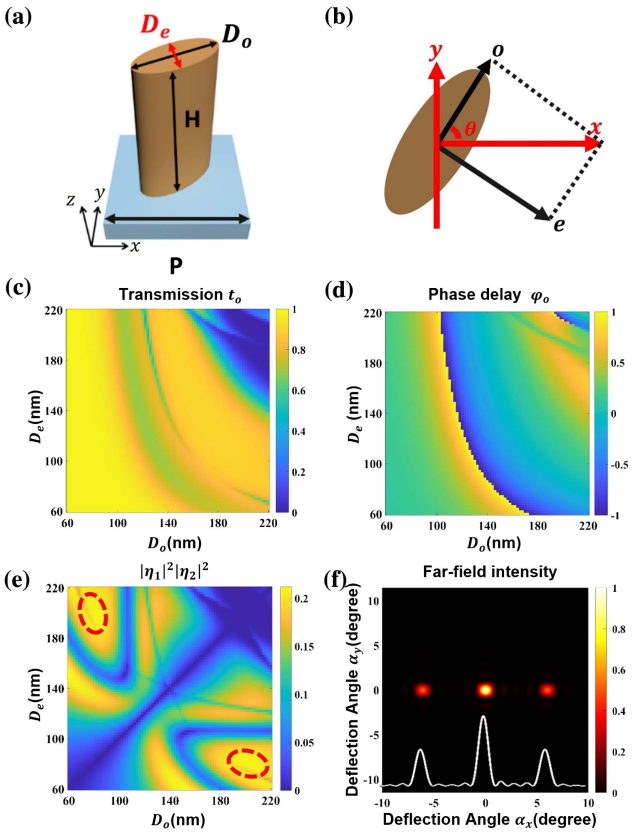

Fig. 2. The design of the displacement measurement metasurface. (a) The perspective view of the unit cell consists of the Si elliptical cylinder located on the quartz. (b) The top view of the nanopillar. (c), (d) The amplitude transmittance t_o and phase delay φ_o for incidence along o axis as a function of D_o and D_e. t_e and φ_e also can be obtained by exchanging D_o and D_e. (e) The maximum interference intensity $|\eta_1|^2|\eta_2|^2$ as a function of D_o and D_e. The region marked by the red dashed ellipse indicates the area with higher intensity and good tolerance for the size of structure. (f) The simulated farfield intensity distribution of a 30 μm × 30 μm metasurface. The bottom is the normalized intensity distribution along α_y = 0°.

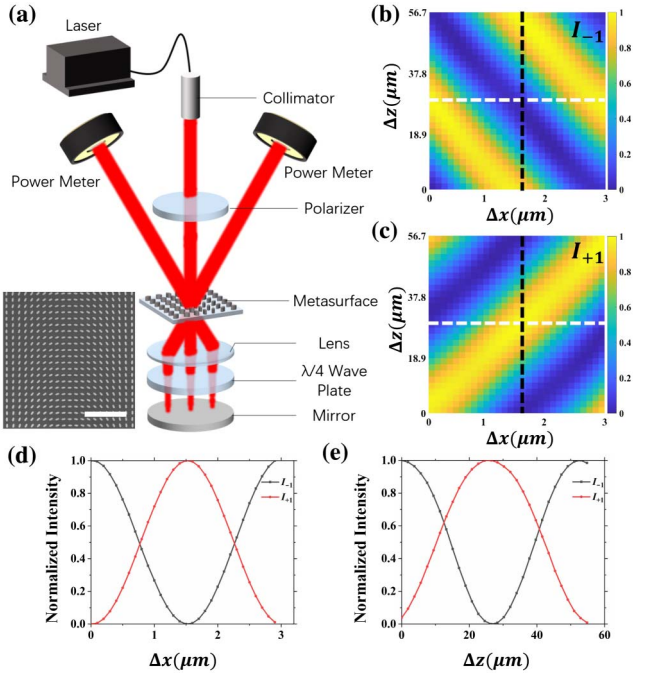

Fig. 3. The displacement measurement properties of the designed metasurface. (a) Schematic illustration of the measurement setup. The inset is the SEM image of the sample. Scale bar, 2 μm. (b), (c) The normalized interference intensity for −1st and +1st order output light as a function of the transversal displacement Δx and the longitudinal displacement Δz. (d) The intensity profiles for −1st and +1st order output light along the white dashed line in (b) and (c). (e) The intensity profiles for −1st and +1st order output light along the black dashed line in (b) and (c).

order beams are measured by two power-meters, respectively. Notably, instead of using two cascaded metasurfaces, only one metasurface and a mirror are employed in the setup, which simplifies the optical path and avoids the fabrication deviation for two metasurfaces[12]. In this reflective system, the measured displacement corresponds to the distance of the metasurface and its own image. As a result, when the metasurface moves $+\Delta x$ or $+\Delta z$, the image of metasurface moves $-\Delta x$ or $-\Delta z$. Therefore, the measured displacement is effectively doubled, becoming $2\Delta x$ and $2\Delta z$. This configuration enhances the sensitivity of displacement measurement, doubling the sensitivity using two cascading metasurfaces.

In the displacement measurement, we first align the center of the metasurface with the optical axis. Subsequently, a 2D-scan is performed by moving the metasurface along the x-axis with a step size of 100 nm and along the z-axis with a step size of 1.89 μm. The measured intensity signals of −1st and +1st order output light as a function of Δx and Δz are plotted in Figs. 3(b) and 3(c). The measured intensities have been normalized for clear visualization. It is clear that the output intensities vary periodically along two opposite directions, which proves the capability of the metasurface simultaneously detecting two-dimensional displacement. As shown in Figs. 3(d) and 3(e), profiles are drawn along the white and black dashed line in Figs. 3(b) and 3(c) to determine the period of intensity. All profiles are cosinoidal as predicted and can be fitted using $I_x(\Delta x) = \frac{1}{2}[1 - \cos(k_x \cdot 2\Delta x + \varphi_x)]$ and $I_z(\Delta z) = \frac{1}{2}\{1 - \cos[(k - k_z) \cdot 2\Delta z + \varphi_z]\}$ respectively. φ_x (φ_z) is the constant phase arising from the constant Δz (Δx). The fitted intensity period of −1st order output light along the x-axis is 3.02 μm and along the z-axis is 53.3 μm, and these are 2.95 μm and 60.8 μm for +1st order output light. All of the results agree with the theoretical periods $\pi/k_x = 3$ μm and $\pi/(k - k_z) = 56.7$ μm. The deviation between the intensity period of −1st and +1st order beams along the z-axis primarily results from the inclination of the metasurface and the mirror with respect to the horizontal plane. Furthermore, the experimental $|\eta_1|^2|\eta_2|^2$ is 0.113, which is measured by the half of the ratio of the maximum intensity of I_{+1} and I_{-1} to the incident light. The decline of $|\eta_1|^2|\eta_2|^2$ mainly suffers from the fabrication deviation of the metasurface and is also slightly influenced by the absorption of optical components and the calibration of the reflective 4f-system.

To determine the sensitivity of the displacement measurement system, we focus on the linear regions of the intensity curves, where the maximum sensitivity is observed. In these regions, the intensity can be approximated as $I_x(\Delta x) = \frac{1}{2}(1 \pm 2k_x\Delta x)$ and $I_z(\Delta z) = \frac{1}{2}[1 \pm 2(k - k_z)\Delta z]$[11]. The corresponding normalized sensitivities can be obtained by $s_x = |\mathrm{d}I_x/\mathrm{d}\Delta x| = k_x$ and $s_z = |\mathrm{d}I_z/\mathrm{d}\Delta z| = k - k_z$. In the experiment, we perform a scan of the metasurface along the x-axis with a step size of 20 nm. At each position, the output signal is measured within 1 s at a sampling frequency of 500 Hz. The averaged measurement results are shown in Fig. 4(a), where the error bars are the standard deviation of the measured intensity at each position. The fitted curves exhibit the sensitivities of $s_{x,-1} = 1.041\ \mu\mathrm{m}^{-1}$ and $s_{x,+1} = 0.997\ \mu\mathrm{m}^{-1}$ for −1st and +1st order output light, respectively, which are in good agreement with the theoretical sensitivity $s_x = 1.047\ \mu\mathrm{m}^{-1}$. Similarly, a scan of the metasurface along the z-axis is performed with a step of 378 nm as shown in Fig. 4(b). The fitted sensitivities are $s_{z,-1} = 0.0591\ \mu\mathrm{m}^{-1}$ and $s_{z,+1} = 0.0487\ \mu\mathrm{m}^{-1}$ for −1st and +1st order output light, respectively, which also show good agreement with the theoretical sensitivity $0.0554\ \mu\mathrm{m}^{-1}$. It is noted that the linear region can be shifted on demand if we introduce a variable phase delay on the zeroth-order light ($\boldsymbol{E}_0$). Therefore, the linear region can be easily found without pre-positioning for the metasurface.

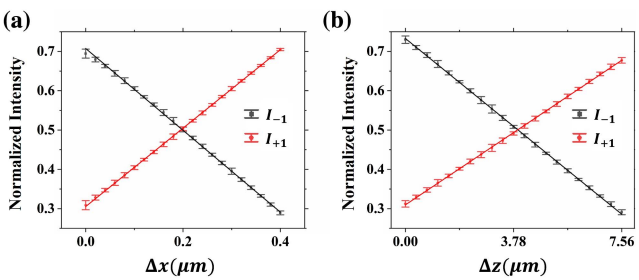

Fig. 4. The sensitivity and resolution of transversal and longitudinal displacement measurement. The linear regions of the (a) transversal and (b) longitudinal displacement measurement.

Finally, we quantify the measurement resolution of our measurement scheme along the x- and z-axes. We examine the average standard deviations of measured intensity along the x-axis in Fig. 4(a), which are $\sigma_{x,-1} = 0.0056$ and $\sigma_{x,+1} = 0.0048$. The clearly resolvable displacement can then be obtained by σ_x/s_x, which is 5.4 nm and 4.8 nm. Similarly, the average standard deviations along the z-axis in Fig. 4(b) are $\sigma_{z,-1} = 0.0056$ and $\sigma_{z,+1} = 0.0059$, and the corresponding resolvable displacements are calculated as 0.095 μm and 0.12 μm. It is worth noting that the measurement resolution can be further improved by enhancing the stability of piezo-stage and reducing ambient noise such as using a more stable optical table or working in an underground laboratory. Additionally, another way to increase the resolution is to reduce the spatial period of the nanopillars Λ. For instance, if Λ is halved to 3 μm, the theoretical sensitivity along the x-axis will increase to $2.094\,\mu m^{-1}$, which is twice the sensitivity of the designed metasurface. The sensitivity along the z-axis will increase to $0.2235\,\mu m^{-1}$, almost quadruple the designed sensitivity. Although it is hard to increase the sensitivity along the z-axis to the same level of sensitivity along the x-axis due to the fabrication challenge, the current measurement resolution is high enough to meet the requirement of some applications such as microelectromechanical systems (MEMS)[26] and the laser direct-write (LDW) technique[27].

4. Discussion

In summary, we proposed and experimentally demonstrated a displacement measurement device by a dielectric metasurface, which can precisely measure transversal and longitudinal displacement simultaneously. By measuring the interference optical intensity of the deflected light beams from the metasurface, transversal and longitudinal displacement of the metasurface can be accurately obtained. The experimental measurement clearly resolved displacements down to 5.4 nm along the x-axis and 0.12 μm along z-axis. The measurement precision can be further improved by reducing the spatial period of the nanopillars and enhancing experimental conditions. Our work opens up new possibilities for compact multidimensional displacement sensing and has potential applications in multiple fields including nanofabrication or microscopy.

Acknowledgements

This work was supported by the National Natural Science Foundation of China (No. U20A20216) and the Technology Domain Fund of 173 Project (No. 2021-JCJQ-JJ-0284). This work was partially carried out at the USTC Center for Micro and Nanoscale Research and Fabrication.

References

1. A. J. den Boef, "Optical wafer metrology sensors for process-robust CD and overlay control in semiconductor device manufacturing," Surf. Topogr. Metrol. Prop. **4**, 023001 (2016).
2. N. G. Orji, M. Badaroglu, B. M. Barnes, *et al.*, "Metrology for the next generation of semiconductor devices," Nat. Electron. **1**, 532 (2018).
3. M. Krieg, G. Flaschner, D. Alsteens, *et al.*, "Atomic force microscopy-based mechanobiology," Nat. Rev. Phys. **1**, 41 (2019).
4. B. Huang, M. Bates, and X. W. Zhuang, "Super-resolution fluorescence microscopy," Annu. Rev. Biochem. **78**, 993 (2009).
5. T. Zang, H. Zang, Z. Xi, *et al.*, "Asymmetric excitation of surface plasmon polaritons via paired slot antennas for angstrom displacement sensing," Phys. Rev. Lett. **124**, 243901 (2020).
6. A. Bag, M. Neugebauer, P. Woniak, *et al.*, "Transverse Kerker scattering for angstrom localization of nanoparticles," Phys. Rev. Lett. **121**, 193902 (2018).
7. Z. Xi and H. Urbach, "Magnetic dipole scattering from metallic nanowire for ultrasensitive deflection sensing," Phys. Rev. Lett. **119**, 053902 (2017).
8. G. H. Yuan and N. I. Zheludev, "Detecting nanometric displacements with optical ruler metrology," Science **364**, 771 (2019).
9. Z. Xi, L. Wei, A. J. L. Adam, *et al.*, "Accurate feeding of nanoantenna by singular optics for nanoscale translational and rotational displacement sensing," Phys. Rev. Lett. **117**, 113903 (2016).
10. Z. Xi, S. Konijnenberg, and H. Urbach, "Information-efficient metagrating for transverse-position metrology," Phys. Rev. Appl. **14**, 014026 (2020).
11. R. Barboza, A. Babazadeh, L. Marrucci, *et al.*, "Ultra-sensitive measurement of transverse displacements with linear photonic gears," Nat. Commun. **13**, 1080 (2022).
12. H. Zang, Z. Xi, Z. Zhang, *et al.*, "Ultrasensitive and long-range transverse displacement metrology with polarization-encoded metasurface," Sci. Adv. **8**, eadd1973 (2022).
13. T. Saucedo, M. H. De la Torre-Ibarra, F. M. Santoyo, *et al.*, "Digital holographic interferometer using simultaneously three lasers and a single monochrome sensor for 3D displacement measurements," Opt. Express **18**, 19867 (2010).
14. H. Yan and B. Pan, "Three-dimensional displacement measurement based on the combination of digital holography and digital image correlation," Opt. Lett. **39**, 5166 (2014).
15. L. Felipe-Sese, P. Siegmann, F. A. Diaz, *et al.*, "Simultaneous in-and-out-of-plane displacement measurements using fringe projection and digital image correlation," Opt. Laser. Eng. **52**, 66 (2014).
16. M. H. Ortiz and E. A. Patterson, "Location and shape measurement using a portable fringe projection system," Exp. Mech. **45**, 197 (2005).
17. B. Pan, D. F. Wu, and Y. Xia, "Incremental calculation for large deformation measurement using reliability-guided digital image correlation," Opt. Laser. Eng. **50**, 586 (2012).
18. T. Saucedo Anaya, M. De la Torre, and F. Mendoza Santoyo, "Microstrain detection using simultaneous endoscopic pulsed digital holography," Opt. Eng. **47**, 073601 (2008).
19. P. J. de Groot, V. G. Badami, and J. Liesener, "Concepts and geometries for the next generation of precision heterodyne optical encoders," in *Proceedings of the Annual Meeting of the American Society for Precision Engineering* (2016), p. 23.
20. D. M. Lin, P. Y. Fan, E. Hasman, *et al.*, "Dielectric gradient metasurface optical elements," Science **345**, 298 (2014).
21. J. B. Mueller, N. A. Rubin, R. C. Devlin, *et al.*, "Metasurface polarization optics: independent phase control of arbitrary orthogonal states of polarization," Phys. Rev. Lett. **118**, 113901 (2017).
22. C. Menzel, C. Rockstuhl, and F. Lederer, "Advanced Jones calculus for the classification of periodic metamaterials," Phys. Rev. A **82**, 053811 (2010).
23. M. K. Chen, X. Liu, Y. Wu, *et al.*, "A meta-device for intelligent depth perception," Adv. Mater. **35**, 2107465 (2023).
24. J. Yao, R. Lin, M. K. Chen, *et al.*, "Integrated-resonant metadevices: a review," Adv. Photonics **5**, 024001 (2023).
25. M. K. Chen, X. Liu, Y. Sun, *et al.*, "Artificial intelligence in meta-optics," Chem. Rev. **122**, 15356 (2022).
26. J. W. Judy, "Microelectromechanical systems (MEMS): fabrication, design and applications," Smart Mater. Struct. **10**, 1115 (2001).
27. C. B. Arnold, P. Serra, and A. Piqué, "Laser direct-write techniques for printing of complex materials," MRS Bull. **32**, 23 (2007).